Materials & Design 225 (2023) 111594

Contents lists available at ScienceDirect

Materials & Design

journal homepage: www.elsevier.com/locate/matdes

Mechanical performances of the interface between the substrate and deposited material in aluminium wire Direct Energy Deposition

E. Eimer [a,*], S. Williams [a], J. Ding [a], S. Ganguly [a], B. Chehab [b]

[a] Cranfield University, College Road, Cranfield, Wharley End, Bedford MK43 0AL, United Kingdom
[b] Constellium Technology Centre, 725, Rue, Aristide, Berges, 38341 Voreppe, France

HIGHLIGHTS

- The mechanical properties of the un-rolled and non-heat treated deposit in this work are lower than the substrate.
- Heat treatment increases and homogenises the properties at the interface, but compromises are required if the wire and substrate do not have the same chemical composition.
- When using different alloys for the wire and substrate, there is a variation of chemical composition across the interface that can promote the formation of microcracks or increase the hardness locally.
- Interlayer rolling reduces the difference in strength between the substrate and Wire + Arc Additive Manufacture deposit and reduces the formation of micro-cracks at the interface.

GRAPHICAL ABSTRACT

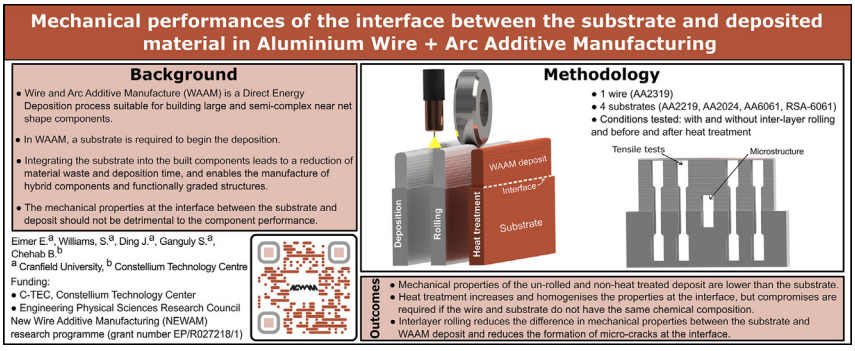

ARTICLE INFO

Article history:
Received 7 July 2022
Revised 16 December 2022
Accepted 2 January 2023
Available online 4 January 2023

Keywords:
WAAM
Additive manufacturing
Hybrid
Aluminium
DED

ABSTRACT

Wire and Arc Additive manufacturing (WAAM) is a Direct Energy Deposition process suitable for the manufacture of large aluminium components. Additive Manufacturing can enable the production of functionally graded structure which could be done by integrating the substrate required to start the deposition into the final component. This paper aims to assess the possibility of including a substrate in a component by investigating the mechanical performances of the interface between a wrought plate and WAAM deposit. Four substrates alloys and 2319 WAAM alloy were investigated. Inter-layer rolling and heat treatment, process steps known for improving the properties of WAAM deposit, were implemented. Each interface was examined using microhardness profiles, tensile tests, post rupture fractography and microstructural analysis. The WAAM deposit hardness was lower than that of the substrate in the as-deposited condition. Although the interface had no impact when using the same alloy for both substrate and wire, the weakest point of the combination was at the interface in dissimilar alloy

* Corresponding author.
E-mail address: e.eimer@cranfield.ac.uk (E. Eimer).

https://doi.org/10.1016/j.matdes.2023.111594

combination. Heat treatment reduced the properties difference between the substrate and WAAM deposit. Inter-pass rolling strengthen the WAAM deposit without impacting the substrate and eliminated the micro crack that occasionally formed in the fusion zone in the as-deposited condition.

1. Introduction

The need for functionally graded components comes from the limitation of material performances and extreme environments. The first use of parts made of multiple materials was reported in the 1980s by a Japanese team who needed to manufacture a component that can work under an extremely high thermal gradient [1]. Functionally Graded Materials (FGMs) can be very beneficial in extreme environments, where high mechanical performances are required along with resistance toward corrosion, radiation, wear rate, or temperature. Additive Manufacturing (AM) processes are well known for their potential of production of FGMs [2-6]. A wide range of papers has been published on hybrid manufacturing, which consists of combining AM and conventional processes to manufacture functionally graded structures. For instance, Merklein et al. [7] combined laser direct metal deposition, laser cutting, deep drawing and upset forging processes to demonstrate the advantage of such an integrated manufacturing route to produce functional gear components.

Aluminium alloys are widely used in the aerospace sector because of their high specific strength, damage tolerance, and corrosion resistance properties. However, different series of aluminium alloys have a wide range and varying properties and are used in different parts of an aircraft. For instance, aluminium copper alloys are commonly used in the lower part of aeroplane wings, where damage tolerance is the most critical design factor. However, aluminium zinc alloys are usually found in the top section, where strength is the primary requirement [8]. Therefore, the use of aluminium FGMs in this sector is of great interest.

Wire and Arc Additive Manufacturing (WAAM), described by Williams et al. [9], is an AM process that uses an electric arc as the heat source and wire as feed material. It is suitable for large scale component manufacturing due to its high deposition rate and the possibility of depositing in an open architecture using local shielding [10]. Given the nature of the process, it requires a substrate to start the deposition. The substrate can be integrated into the final design or be sacrificial. Locket et al. [11] detailed that substrate integration is usually the best option to reduce manufacturing difficulty and cost. FGMs can be produced using the same alloy and exploiting the different microstructures of the substrate and WAAM deposit or using two different alloys. To integrate the substrate into a WAAM part, the properties of the interface between the substrate and the WAAM deposit ideally needs to be at least as good as the rest of the component. However, little is known about the properties of the interface between WAAM deposit and substrate. Zhang et al. [12] studied the fatigue behaviour of a Ti6Al4V interface; Gu et al. [13] investigated the microstructure and tensile properties of aluminium interfaces focusing on the effect of deposition parameters and post deposition heat treatment. Eimer et al. [14] reported microstructure observation of the interface between aluminium deposit and four 2000 series aluminium alloys, but no mechanical testing was carried out.

Aluminium alloys have proven suitable for WAAM with various chemical compositions; of particular interest is the 2319 alloy [15-20]. This alloy is relevant to the aerospace sector as it is currently used to weld propellant tanks. Gu et al. showed how this alloy performs and how its properties can be improved by heat treatment and inter-pass rolling [15,16]. Honnige et al. [21] demonstrated the effect of the deposition on a substrate, under different inter-pass rolling conditions, on the residual stress profiles and distortions. This alloy was chosen as the WAAM deposit in the study presented here. This paper aims to assess the possibility of integrating the substrate in an aluminium WAAM component. Several phenomena are well known from welding metallurgy, including softening of the Heat Affected Zone (HAZ) [22,23], alloying element segregation in the partially melted zone [24-26], and hot cracking in the fusion zone [27-29], could affect the mechanical performance of the interfaces, as reported by Eimer et al. [14].

Four different substrates with different aluminium alloys were used to overview the effect of alloy combinations and process conditions on the interface performances.

- 2219 and 2024 substrate alloys were selected as they are widely used for structural applications [30, pp. 3-67/3-69]. 2219 is particularly interesting as its composition is similar to the 2319 filler wire selected for this work. The study of the 2219 substrate and 2319 WAAM deposit combination enabled a focus on microstructural features, while the 2024 substrate and 2319 WAAM combination provided an outlook on challenges occurring when using dissimilar alloys.
- As shown in previous work [14], the substrate microstructure, especially grain size, can impact defect formation in the partially melted zone. To investigate this phenomenon on the mechanical performance, two substrates made of the same alloy were selected, one conventionally made and one rapidly solidified. 6061 is an alloy commonly used for cryogenic applications requiring high toughness [30, pp.3–250] and is available in rapidly solidified and rolled conditions. It was therefore selected for this part of the investigation.

In addition to four different substrates, four processing conditions, including as-deposited, inter-pass rolled, heat treated, and rolled + heat treated, were used to produce samples for mechanical testing.

2. Methodology

One filler wire, AA 2319, was deposited on four different substrates, mentioned in Table 1, to manufacture the specimens studied. The chemical compositions of the filler wire and substrate are shown below in Table 1. The RSA-6061 was manufactured using a melt-spinning technology that ensures an exceptionally high cooling rate and results in small grain sizes [31]. It was compared to a substrate made conventionally with the same alloy, called 6061_{Rolled} in the paper.

The filler wire was deposited on the edge of the substrate, as illustrated in Fig. 1. The WAAM deposit was produced as a single bead wall 200 mm long and 50 mm high. In this paper, the Substrate alloy + filler wire was used for nomenclature. For instance, the combination between 2219 substrate and 2319 WAAM deposit is called 2219+2319.

The pulsed Cold Metal Transfer (CMT) process, a relatively high input CMT mode developed by Fronius, was used to deposit the first layer on the cold substrate. The subsequent layers were deposited with the CMT Pulse Advance process with a gradual decrease of Wire Feed Speed (WFS) and heat input [17]. The CMT Pulse

Table 1
Chemical composition in weight % [32]

Alloy	Condition	Cu	Mg	Si	Ti	Zr	Fe	Mn	V
2319	Wire	5.8-6.8	Max 0.02	Max 0.20	0.10-0.20	0.10-0.25	Max 0.30	0.20-0.40	0.05-0.15
2219	Substrate (Rolled - T8)	5.8-6.8	Max 0.02	Max 0.20	0.02-0.10	0.10-0.25	Max 0.30	0.20-0.40	0.05-0.15
2024	Substrate (Rolled - T3)	3.7-4.5	1.2-1.5	Max 0.15	Max 0.15	...	Max 0.20	0.15-0.8	...
6061_{Rolled}	Substrate (Rolled - T6)	0.15-0.40	0.8-1.2	0.40-0.8	Max 0.15	...	Max 0.7	Max 0.15	...
RSA-6061	Substrate (Spined-cooled - T6)	0.15-0.40	0.8-1.2	0.40-0.8	Max 0.15	...	Max 0.7	Max 0.15	...

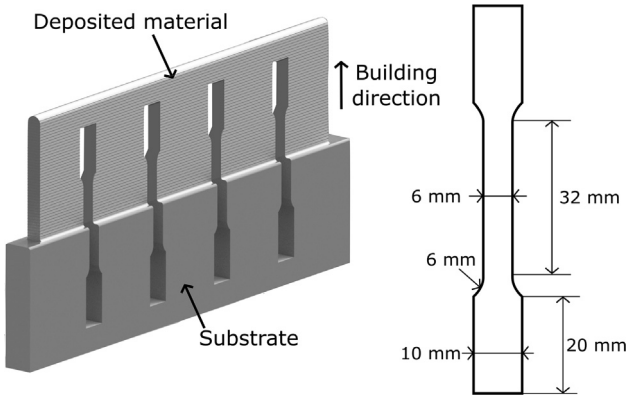

Fig. 1. Diagram of the material deposited and extraction zone for tensile test and microstructure study. The tensile specimen thickness was 2.5 mm.

Advance process was chosen due to the low porosity level it generates in the deposit [33] and the process parameters based on a previous study on 2319 WAAM [15]. The process parameters are provided in Table 2. The start and stop position were alternated every layer. For the inter-pass rolled material, a 100 mm diameter roller was used to apply pressure generated by a hydraulic cylinder. The set-up used was previously described by Gu et al. [15]. A rolling load of 45 kN was used with a roller travel speed of 10 mm/s 30 seconds after the layer deposition.

During heat treatment, the samples were solutionised at 535°C for 90 minutes, water quenched, and artificially aged at 175°C for three hours, as suggested in Gu et al. study [15]. This aging duration was selected so the results could be compared to the literature on 2319 WAAM. Heat treatment was carried out for the 2219+2319 and 6061+2319 combinations as these alloys have the same solution treatment temperature. The issues occurring during the heat treatment of the 2024+2319, due to the low melting point of the 2024 alloys were previously reported [14]

The tensile specimens were machined, as shown in Fig. 1. Coupons were also taken from the substrates and WAAM deposit to evaluate the mechanical properties in these areas in as-deposited or as-received conditions and after heat treatment. The tensile tests were carried out following the ASTM B557M standard at a constant displacement of 1mm/min. In most cases, the test was monitored using a laser extensometer that only recorded the gauge length extension. In addition, the specimen taken from the combinations 6061+2319 were measured using a Digital Image Correlation (DIC) device. This technique enabled the recording of spatially resolved stress-strain behaviour of the graded specimens. The samples were sprayed with a black and white pattern, and two cameras monitored the evolution of this pattern. The software instra4D was used to calibrate the camera set up and produce localised strain measurement with a resolution of 340µm across the specimens. A Matlab code was developed to analyse the raw DIC data and determine the localised yield strength across the gauge length. In addition, microhardness profiles were measured along the centre line in the cross section of the samples using a load of 200 g and an indentation holding time of 15s with a Zwick/Roell machine. In the micro-hardness profiles presented in this paper, the location of the substrate, fusion zone, and deposited material is shown. The position of these areas was determined using microstructural observations.

The ruptured tensile specimens and interface cross-sections were mounted, ground using grit SiC papers under flowing water and polished to a mirror finished surface with 6 and 3 µm diamond paste and colloidal silica suspension. The samples were etched using Keller's reagent, and the micrographs were taken with an Optiphot Nikon optical microscope. An XL30 Scanning Electron Microscope (SEM) with an X-MAXN detector was used for Energy-dispersive X-ray Spectroscopy (EDS).

3. Results

3.1. 2219 substrate with 2319 WAAM deposit (further referred to as 2219+2319)

Fig. 2 shows the hardness profile across the interface between 2219 substrate and 2319 WAAM deposit under four different conditions. In the as-deposited condition, the hardness of the WAAM deposit was significantly lower than the substrate hardness. The hardness transition was relatively smooth apart from a transition step between 90HV and 70HV at the fusion line. When inter-pass rolling was carried out, the hardness of the WAAM deposit and fusion zone increased. However, the hardness of the fusion zone was slightly lower than this of the deposited material. The lower effectiveness of rolling on the fusion zone due to the geometrical constraint of the substrate could be the origin of this hardness difference with the WAAM deposit. The heat-treated profiles were stable and not impacted by inter-pass rolling.

Table 3 provides the tensile properties of the 2219 substrate, 2319 WAAM deposit and 2219 + 2319 interface; the data taken from the literature is provided along with a reference. The tensile

Table 2
Process parameters.

Layer	1	2-3	4-5	from 6
Process	CMT Pulse	CMT Pulse Advanced		
WFS [m/min]	7	9	7.5	6
TS [mm/s]	10			
Workpiece to tip distance [mm]	13			
Shielding gas flow rate [L/min]	20			
Waiting time [s]	120			

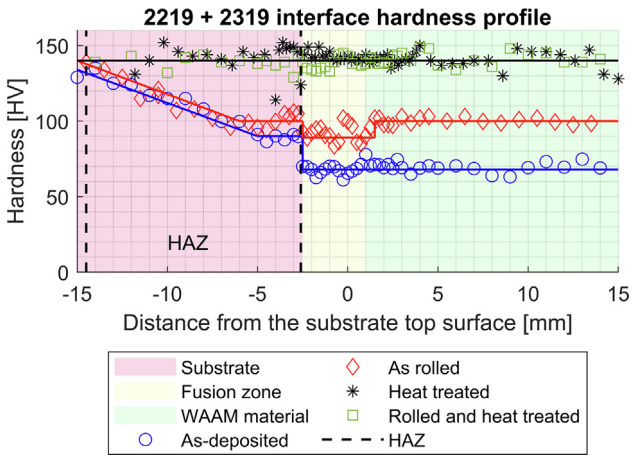

Fig. 2. Effect of inter-pass rolling and heat treatment on the hardness (HV0.2) profile across the 2219 + 2319 interface

Table 3
Tensile properties of the 2219+2319 interface

Conditions	0.2% PS [MPa]	UTS [MPa]	Elongation [%]
2219 substrate			
As received (T8)	350 ± 5	450 ± 5	10 ± 1
Heat treated*	245 ± 10	423 ± 5	23 ± 2
2319 WAAM deposit			
As-deposited [15]	131	259	15.5
heat treated	266 ± 16	370 ± 13	5.3 ± 1.0
Inter-layer rolled [15]	244	311	6.6
Interface 2219 + 2319			
As-deposited	118 ± 8	257 ± 13	8.5 ± 1.5
Inter-layer rolled	224 ± 21	270 ± 18	2.2 ± 0.7
Heat treated	270 ± 18	355 ± 12	3.5 ± 0.7
Inter-layer rolled and heat treated	272 ± 22	362 ± 26	4 ± 2

* Same heat treatment to the one applied to the interface as described in the methodology section.

properties of the interface were measured using the coupons shown in Fig. 1. The properties of the substrate were measured using coupons extracted in the substrate only, parallel to the interface specimens. Under the as-deposited condition, the interface's 0.2% Proof Stress (PF) and Ultimate Tensile Strength (UTS) were similar to those of the 2319 WAAM deposit reported by Gu et al.. However, the elongation was significantly lower than that of as-deposited material. Inter-pass rolling increased the 0.2% PS of the interface but had little effect on the UTS and considerably reduced the elongation compared with the as-deposited condition. A high local concentration of defects often causes such a phenomenon in materials.

Prior to heat treatment, the rolled interface properties reached a similar 0.2% PS, but the UTS and elongation were lower than that of the rolled WAAM deposit. In this case, the true UTS could not be measured because of the premature rupture of the coupons. The value reported as UTS is the strength at rupture. Heat treatment increased the 0.2% PS and UTS but reduced the elongation. Under the heat-treated condition, the interface results were similar to the heat-treated WAAM deposit results, with a lower elongation. The properties of the heat-treated interfaces were not impacted

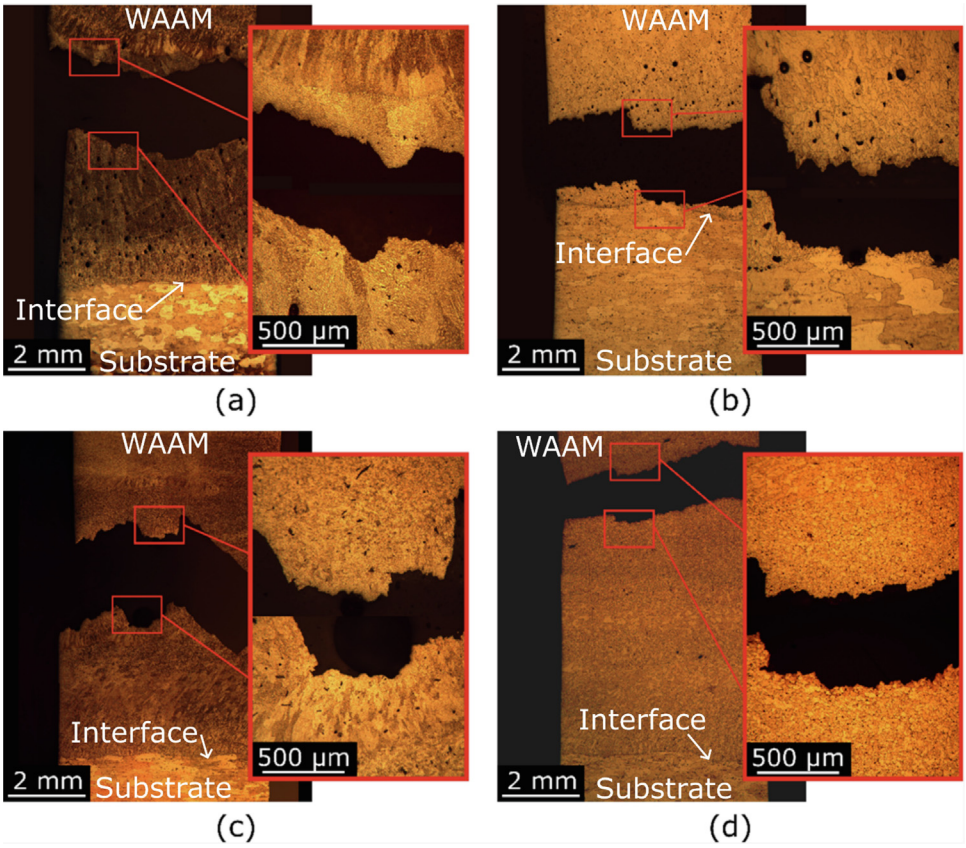

Fig. 3. Optical images of broken tensile specimens representative of the (a) as-deposited (un-rolled and non-heat treated), (b) heat treated, (c) inter-pass rolled, and (d) inter-pass rolled & heat treated.

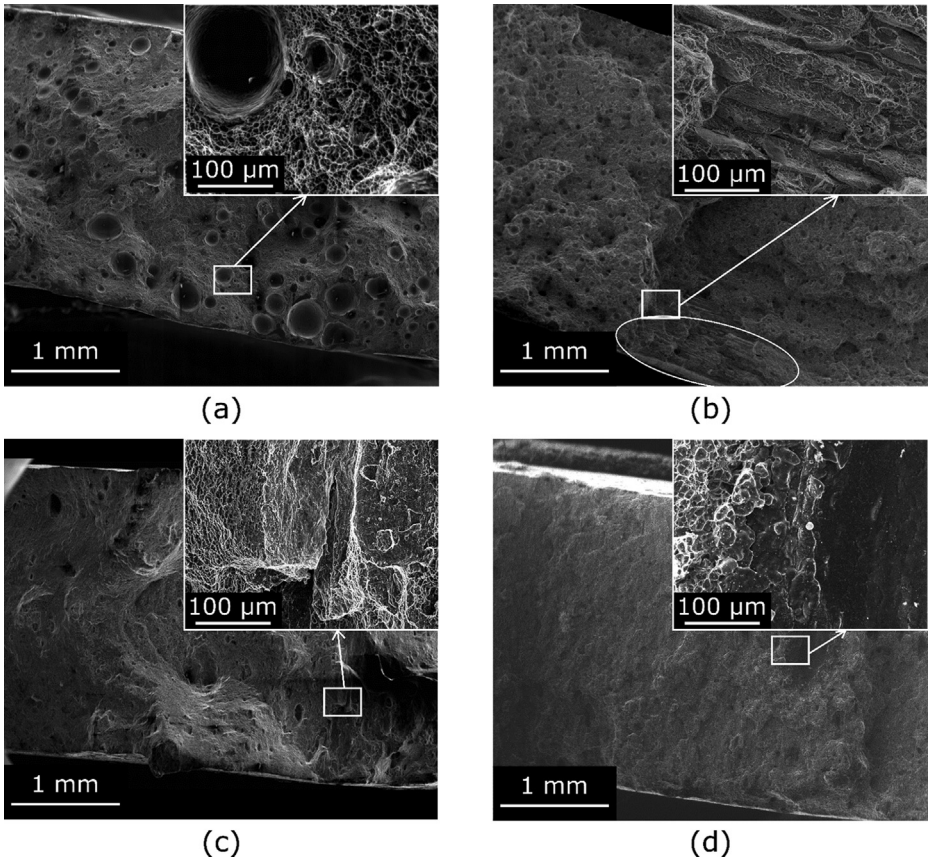

Fig. 4. Fracture surface of specimens in the (a) as-deposited, (b) heat treated, (c) inter-pass rolled, and (d) inter-pass rolled & heat treated

by inter-pass rolling. The 0.2% PS and UTS of the 2219 substrate were higher than those of the interface, regardless of the conditions.

Fig. 3 shows optical images of the ruptured tensile specimens of the 2219+2319 interfaces under four conditions. In the as-deposited and as-rolled states, the rupture occurred in the first layer of the deposited material. The rupture occurred at the fusion boundary between the substrate and the WAAM deposit for the heat-treated sample. The inter-pass rolled & heat-treated sample ruptured in the WAAM deposit far away from the interface. In Fig. 3(c), the magnified image shows a significantly different microstructure on either side of the rupture, with a colony of large grains in the bottom part of the coupon.

Fig. 4 shows the rupture surfaces of the specimens shown in Fig. 3. A high porosity level was observed in the as-deposited sample, as shown in Fig. 4(a). The fracture surface features were typical for a relatively ductile fracture. Two different microstructures were observed in the heat-treated specimen in Fig. 4, which are from the WAAM deposit, and 2219 substrate (highlighted by the ellipse). The zone consisting of large substrate grains, highlighted in Fig. 4(b), is typical of intergranular rupture showing no evidence of crack propagation resistance. The rupture surface of the rolled specimen, shown in Fig. 4(c), was rough, with numerous defects, typical of a brittle rupture and coherent with the low elongation reported in Table 3. This observation, combined with Fig. 3(c) indicates that uneven microstructure across layer height and un-closed pores may have caused the premature failure of this combination. However, the porosity level was considerably lower than in the as-deposited specimen. The inter-pass rolled & heat-treated rupture surface, shown in Fig. 4(d), was covered in dimples, although some elliptic features which surfaces show no evidence of crack propagation resistance were observed. However, these areas were sparse compared to the as-deposited and as-rolled specimens.

3.2. Multi-material interface

3.2.1. 2024 series substrate

Fig. 5 shows the hardness profile across the 2024+2319 interfaces. In both conditions, the hardness of the WAAM deposit was lower than the hardness of the substrate. However, the gap between the two was reduced by inter-pass rolling. In the as-

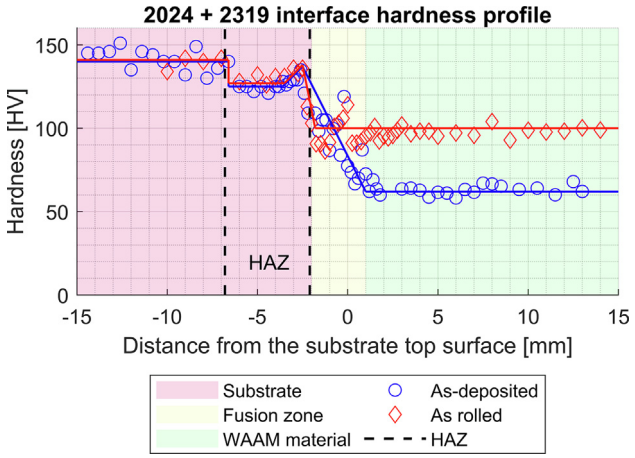

Fig. 5. Hardness profile (HV0.2) across the 2024+2319 interface in as-deposited and inter-pass rolled condition

deposited state, the transition between the substrate and WAAM deposit was not as smooth as observed for the 2219+2319 interface in Fig. 2. The hardness of the fusion zone was higher for the 2024 +2319 compared with the 2219+2319 with average values of 99 HV and 68HV, respectively.

Fig. 6 shows that this high hardness in the fusion zone can be correlated with a slightly higher magnesium content in this area compared to the rest of the WAAM deposit. The 2024 substrate dilution caused this magnesium content during the first bead of 2319 alloy deposition. In the inter-pass rolled status, the hardness of the WAAM deposit is the same as the fusion zone and the first deposited layer. The hardness decrease between the WAAM deposit and substrate occurred in only one step.

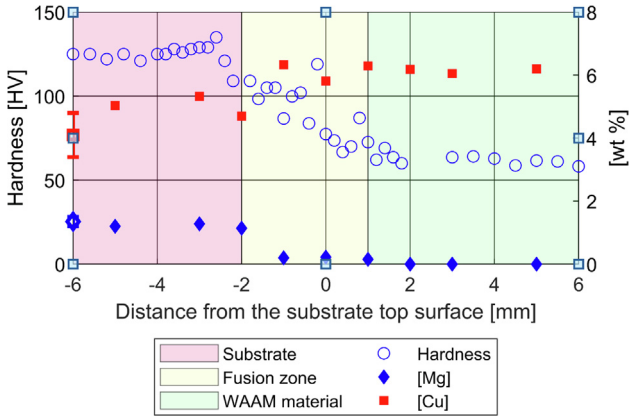

Fig. 6. Hardness profile (HV0.2) across the 2024+2319 as-deposited interface along with local chemical composition measurements. The measurements shown at x=-6 are the chemical composition ranges of the substrate alloy according to the Aluminum Association [32].

Table 4
Tensile properties of the 2024+2319 interface, 2024 substrate and 2319 WAAM deposit.

Conditions	0.2% PS [MPa]	UTS [MPa]	Elongation [%]
2024 substrate			
As received (T3)	364	500	19
2319 WAAM deposit			
As-deposited [15]	131	259	15.5
Inter-layer rolled [15]	244	311	6.6
Interface 2024 + 2319			
As-deposited	147 ± 14	232 ± 12	2.8 ± 0.9
Inter-layer rolled	248 ± 17	270 ± 18	2.2 ± 0.7

Table 4 provides the tensile properties of the 2024+2319 interfaces in both as-deposited and inter-pass rolled conditions. The properties of the as-deposited 2024+2319 were different from the properties of the 2219+2319 given inTable 3. It suggests that the interface impacts the properties of this alloy combination. The 0.2% PS of the 2024+2319 as-deposited interface was slightly higher than the 0.2% PS of the as-deposited WAAM deposit, and the maximum strength measured was slightly lower. However, the elongation of the interface was significantly reduced. This means that microstructural defects were formed in the 2024 +2319 interface but not in the 2219+2319 combination.

In the inter-pass rolled condition, the 0.2% PS of the 2024+2319 interface increased and was similar to the 0.2% PS of the rolled WAAM deposit. The maximum strength measured increased slightly, but it was still significantly lower than the apparent UTS of the inter-pass rolled WAAM deposit. However, inter-pass rolling had no significant impact on the elongation of the 2024+2319 interface. The inter-pass rolled 2024+2319 interface properties were similar to that of the inter-pass rolled 2219+2319 interface.

Fig. 7 shows the optical images of the ruptured tensile specimens. In the as-deposited condition, the rupture occurred at the boundary between the first and second layers of the WAAM deposit, as shown in Fig. 7(a). Some cracks were observed at the grain boundaries. Numerous cracks, highlighted by arrows, can be seen on the rupture surface SEM image shown in Fig. 8(a). No similar cracks were seen in the rupture surface of the as-deposited 2219+2319 interface shown in Fig. 4(a). Fig. 7(b) shows that the rupture occurred further away from the first bead in the inter-pass rolled condition. The grains were much smaller than those in the as-deposited condition, and no cracks were observed. The absence of dimples in the rupture surface, provided in Fig. 8(b), shows that the material had little resistance to crack propagation.

3.2.2. 6xxx series substrates

The SEM images of the partially melted zone of the 6061+2319 interfaces are shown in Fig. 9. Fig. 9(a) shows how the deposition affected the rolled substrate, segregating alloying elements along a grain boundary. Fig. 9(b) shows the transition between the rapidly solidified substrate and the WAAM deposit; alloying element segregation can be seen in the substrate but is limited to a zone less than 20 μm wide. The substrate also does not contain second phases as large as the 6061 rolled substrate shown in Fig. 9(a).

As shown in the hardness plots in Fig. 10, the difference of the substrate, rolled or rapidly solidified, did not affect the hardness results in the as-deposited condition. The hardness of the WAAM deposit was lower than the hardness of the substrate. Also, a hardness drop could be seen below the fusion line in both cases. This

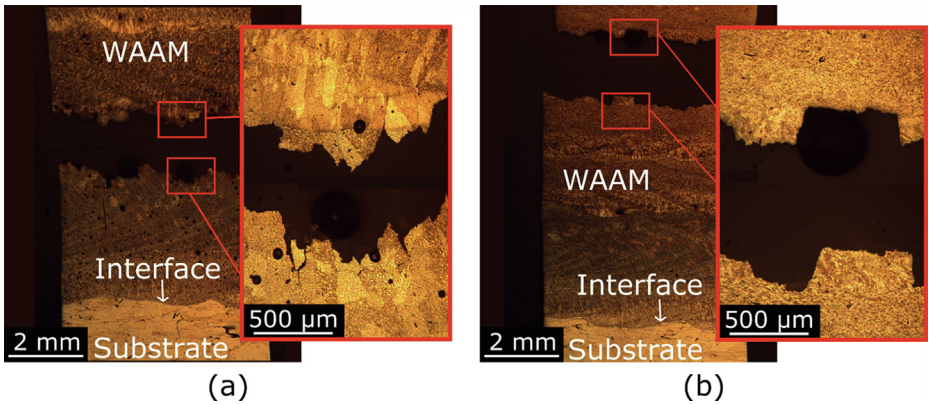

Fig. 7. Ruptured tensile specimen 2024 + 2319 in (a) as-deposited and (b) inter-pass rolled condition

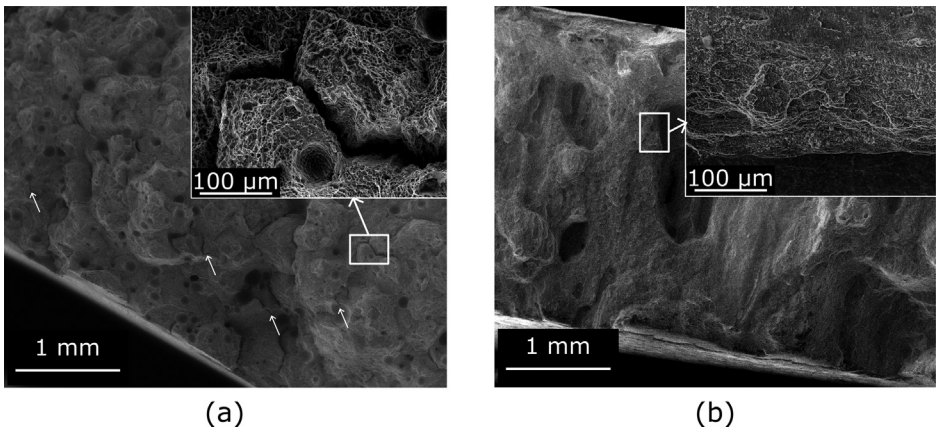

Fig. 8. Rupture surface of the 2024+2319 interfaces in (a) as-deposited and (b) inter-pass rolled conditions.

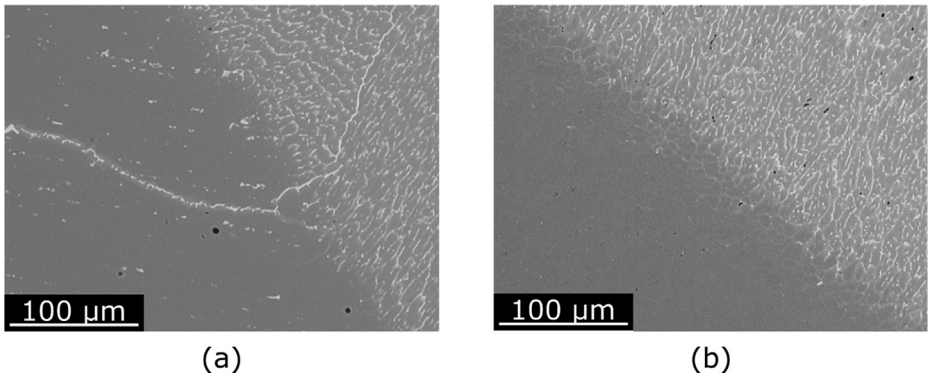

Fig. 9. Partially melted zone of the as-deposited 6061 + 2319 interface using (a) wrought and (b) Rapid solidified substrates.

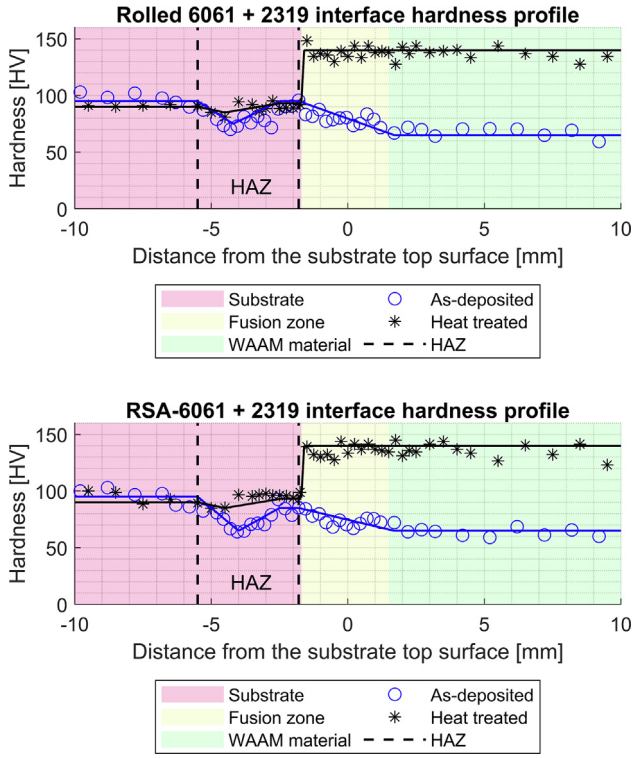

Fig. 10. Hardness profile (HV0.2) of the 6061+2319 interfaces.

reduction in the heat affected zone, typical for 6000 series alloys, is caused by the reversion of β' (Mg_2Si) phases in this zone [23, pp.359–367]. The hardness in the heat affected zone was similar to that of the WAAM deposit. The hardness increased after heat treatment of both rapidly solidified and rolled substrates to a value of 100 HV and 90HV, respectively. In both cases, the hardness drop in the HAZ was considerably reduced but not eliminated, and the hardness of the WAAM deposit was increased significantly. After heat treatment, the WAAM deposit hardness was higher than the substrate hardness, regardless of the nature of the substrate.

Table 5 provides the tensile properties of the 6061+2319 interfaces. In both the as-deposited and heat treated conditions, the properties depended on the nature of the substrate. The 0.2% PS

Table 5
Tensile properties of the 6061+2319 interface, 6061 substrates and 2319 WAAM deposit.

Conditions	0.2% PS [MPa]	UTS [MPa]	Elongation [%]
6061 substrate			
6061_{Rolled} As received (T6)	350 ± 5	450 ± 5	10 ± 1
RSA-6061 As received (T6)	245 ± 10	423 ± 5	23 ± 2
2319 WAAM deposit			
As-deposited [15]	131	259	15.5
Heat treated	266 ± 16	370 ± 13	5.3 ± 1.0
Interface 6061 + 2319			
As-deposited– 6061_{Rolled}	124 ± 21	208 ± 18	5.9 ± 2.6
As-deposited- RSA-6061	148 ± 18	225 ± 10	6.9 ± 0.2
Heat treated – 6061_{Rolled}	168 ± 7	280 ± 2	20.0 ± 0.2
Heat treated – RSA-6061	209 ± 12	328 ± 7	16.6 ± 1.1

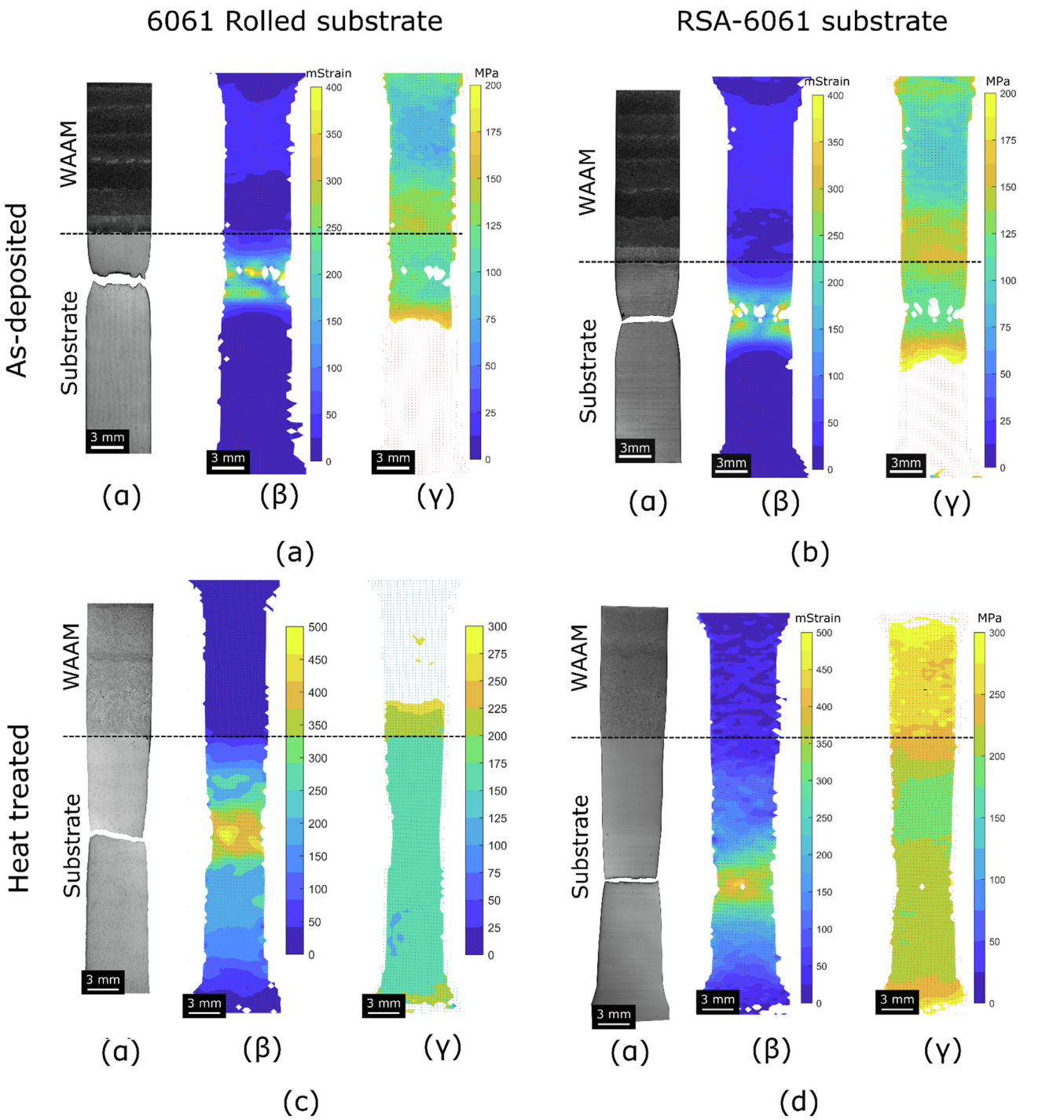

Fig. 11. Digital image correlation results for as-deposited with (a) rolled and (b) RSP substrates and after heat treatment with (c) rolled and (d) RSP substrates. For each case, (α) the optical images of a ruptured tensile specimen, (β) the evaluated strain map before rupture, and (γ) the calculated 0.2% PS maps are displayed.

and UTS of the sample built on the rapidly solidified substrate were significantly higher, but the elongation was slightly lower after heat treatment. In the as-deposited condition, the measured properties were lower than those achieved by the substrates in the as-received conditions according to the substrate supplier [31]. Heat treatment significantly improved the 0.2% PS and UTS and drastically improved the elongation. The 0.2% PS of the heat treated was much lower than the 0.2% PS of the substrate in the as-received state, indicating the treatment adapted to the 2319 deposit, according to Gu et al. [15], is not optimum for the 6061 substrates.

Fig. 11 shows the digital image correlation results for both 6061 +2319 interfaces in as-deposited and heat treated conditions. In all the cases, the rupture occurred in the substrate. The rupture occurred about 3 to 4 millimetres away from the fusion line in the as-deposited condition. That is coherent with the hardness profile, indicating that the hardness was lower in this heat affected zone. The as-deposited specimens can be divided into four zones:

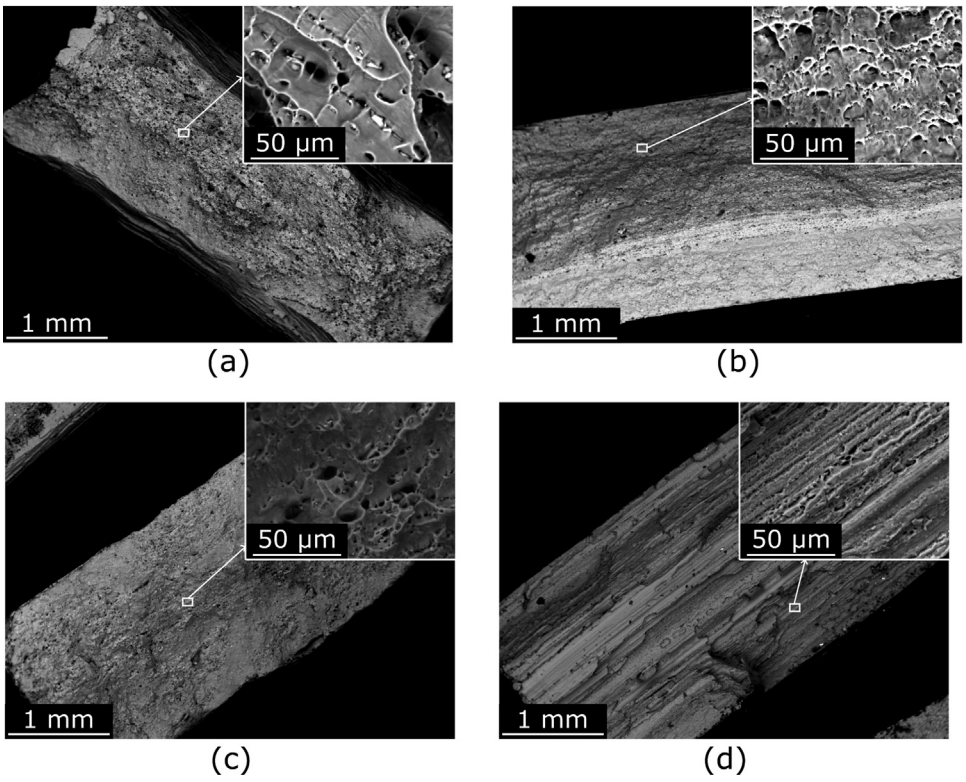

Fig. 12. Rupture surface of the as-deposited (a) 6061_{rolled}+2319 and (b) RSA-6061+2319, and heat treated (c) 6061_{rolled}+2319 and (d) RSA-6061+2319 interfaces

- The WAAM deposit was slightly strained during the test and had the lowest 0.2% PS of all four areas, with a value of around 100 MPa.
- The fusion zone and the first layer of the WAAM deposit were lightly strained and characterised by a higher 0.2% PS, around 140 and 160 MPa for the 6061_{Rolled}+2319 and RSA-6061+2319 interfaces, respectively.
- The heat affected zone was the most strained area and reached a 0.2% PS of around 110 MPa.
- The substrate was not strained to the required level during the test to calculate the 0.2% PS of the parent alloy.

The behaviour of the heat-treated specimens was affected by the substrate type:

- In the RSA-6061+2319 case, the maximum strength measured was 328 MPa, higher than the 0.2% PS calculated in the WAAM deposit (around 275MPa). This means that the stresses were high enough during the test to generate plastic deformation in the WAAM deposit, and it was possible to determine the local 0.2% PS across the whole specimen, as shown in Fig. 11(d) (γ).
- In the 6061_{Rolled}+2319 case, the UTS was 280 MPa, just above the 0.2% PS of the heat treated WAAM deposit. This means that the stresses during the test were not high enough to generate plastic deformation in the WAAM deposit, and it was not possible to determine the 0.2% PS in the WAAM deposit, as shown in Fig. 11(c) (γ).

Fig. 12 shows the rupture surfaces of the 6061+2319 interfaces in both as-deposited and heat treated conditions. The features found on the rupture surfaces were typical of a ductile fracture in both conditions. Elongated features covered most of the rupture surface of the heat treated RSA-6061 substrate.

4. Discussion

4.1. Similar alloy interface

Using the same alloy for both substrate and filler wire produces a relatively smooth transition between the two parts of the interface without any chemical composition variation. The 0.2% PS and UTS of the interface were similar to those reported for WAAM 2319 as-deposited material [15] but with a lower elongation. This reduced elongation can be explained by the absence of plastic deformations in the substrate part of the specimens, as the UTS of the WAAM deposit is lower than the 0.2% PS of the substrate in the as-received condition. Gu et al. [13] reported an elongation of 13.5 to 15% for the interface between 2219 substrate and 2319 WAAM deposit. The difference in as-deposited mechanical properties between this later study [13] and the one presented here can be explained by the intrinsic variability of WAAM deposit due to variation in wire physical quality resulting in variable porosity levels [20,34].

The mechanical properties of this combination were equivalent to the properties of its weakest component, according to Table 3, the WAAM deposit. The UTS and 0.2% PS of the interface were comparable to the UTS and 0.2% PS of the deposit. Therefore, the interface did not affect the strength of the specimens.

To increase the properties of the WAAM deposit, and therefore the interface, three strategies were implemented:

- Inter-pass rolling

The inter-pass rolled 2219+2319 combination properties were similar to the inter-pass rolled WAAM deposit properties, with a 0.2% PS but a lower maximum strength measured [15]. The numerous defects observed in the fracture surface could explain this

lower maximum strength measured, especially as no pores were reported by Gu et al. for the inter-pass rolled WAAM deposit. However, the same authors observed partially closed pores in the cold worked samples using lower rolling load [16]. Also, the drop in the hardness profile from the substrate to the WAAM deposit, shown in Fig. 2, shows that the strengthening of the first deposited layers was not optimum. This, combined with the presence of what seems to be unclosed pores, suggests that inter-pass rolling was not as effective in the first deposited layers as in the rest of the wall. Determining the cause of this phenomenon would require further investigation. However, just as it is required to adapt the deposition parameters for the bottom of a wall to compensate for the heat losses, it would also seem to be appropriate to adjust the cold working parameters based on the vicinity of a layer to the substrate.

- Heat treatment

After heat treatment, the hardness profile was flat, as observed previously [14]. However, both substrate and WAAM deposit tensile test results differed, indicating that they responded differently to heat treatment. The tensile properties of the interface were equivalent to those of the WAAM deposit. Still, the fracture occurred at the fusion line, suggesting that the microstructure changes between the wrought material and WAAM deposit, including grain size, texture, and alloying element distribution, affected the material load response. In this case, the interface is detrimental to the rupture behaviour of the material. These microstructural changes did not initiate the rupture in Gu et al. study [13], and the mechanical properties were reported equivalent to that of the substrate. However, it is essential to highlight that the heat treatment used in the study presented here was identical to that of Gu et al. [15] in their study of the 2319 WAAM deposit. However, in their other publication, the same primary author used a longer ageing duration of the interface between wrought and WAAM deposit [13]. For such alloy, longer ageing duration generates a denser precipitates network [35], increasing the material strength and reducing its ductility, as long as the material is not extensively over-aged. This shows that the ageing duration is critical and should be optimised to achieve the best compromise in terms of substrate and WAAM deposit ageing response.

- Inter-pass rolling & heat treatment

In this condition, the rupture occurred away from the interface. It suggests that, with inter pass rolling, the microstructural changes (grain size, texture, and alloying element distribution) at the fusion line were not as detrimental as in the heat treated interface. The tensile properties of the heat treated interfaces were not affected by the inter-pass cold work, which is similar to the WAAM2319 material as reported by Gu et al. [15]. The fracture occurring somewhere in the deposit rather than at the interface nevertheless demonstrates the benefit of inter-pass rolling.

4.2. Dissimilar alloy interface

4.2.1. 2024 + 2319 interface

The presence of microcracks at the rupture surface indicates that the second bead contained microstructural features, offering no resistance to crack propagation. The chemical composition of 2024 is known to cause unfavourable solidification behaviour during welding [29], making this alloy sensitive to hot cracking. In the case of this study and others [14,36], no hot cracks were observed, as the solidification stresses are believed to be low during free-form WAAM deposition. Constrain during the welding of 2024 plates with 2139 wire have different consequences, as cracks in the second pass have been observed during multi-pass welding of 2024 with 2319 wire by Pickin et al. [27]. This explains the lower ductility of the as-deposited 2024 + 2319 interface compared with the 2219 + 2319 combination. However, no microstructural features susceptible to accelerate crack propagation were observed in the first bead, and inter-pass rolling solved the problem caused by the hot cracking sensitivity of the local chemical composition. The inter-pass rolled interface properties are the same as the inter-pass rolled 2219 + 2319 described in the previous section: nothing specific to the combination 2024 + 2319 affected the tensile properties. However, the hardness drop in the fusion line and first layer observed in the inter-layer rolled 2219 + 2319 interface did not appear in the 2024 + 2319 one. Fig. 6 indicates that the magnesium content in the fusion zone of the 2024 + 2319 combination was significant, and is likely the cause of this high hardness value in this area through solid solution and work hardening. The use of a combination of dissimilar alloys, and the resulting alloying element dilution, has the advantage of increasing the hardness of the fusion zone and the first layer. Controlling the dilution during the first deposited layer can be a suitable way to optimise the mechanical properties of a dissimilar alloy interface.

4.2.2. 6061 + 2319 interface

According to the 0.2% PS map in Fig. 11, the WAAM deposit was weaker than the HAZ in the as-deposited condition, but the rupture occurred there since the HAZ was narrow. The localised strain also caused the low elongation reached by both 6061+2319 interfaces despite the ductile nature of the fracture surface shown in Fig. 12. The partially melted zone shown in Fig. 9 shows that using a substrate with a small grain size reduces liquation issues. This was reported in the literature of fusion welding, showing that using a substrate with small grain reduces alloying element segregation at grain boundaries [26]. It was also reported for the interface between WAAM deposit and substrate [14]. However, due to the resolution of the DIC data, it is not possible to assess the potential benefits of the lack of liquation in the area just beneath the fusion zone on the mechanical properties.

During heat treatment, the properties of the HAZ were partially recovered. This is the expected outcome of the solution treatment. However, the 0.2% PS obtained by the interface was much lower than the 0.2% PS of the substrate in the as-received condition. This suggests that the heat treatment is not optimum for the HAZ. As indicated by the hardness plot in Fig. 10, the gap of mechanical properties between the WAAM deposit and the substrate is lower for the rapidly solidified substrate compared to the rolled one. During the test of the combination using RSA-6061 substrates, the whole coupon was strained while no plastic strain was measured in the WAAM deposit section of the interfaces, including 6061_{Rolled}. This shows the advantage of using a combination of materials with close mechanical properties to reduce strain localisation.

5. Conclusion

This study investigated the effect of alloy combinations and process conditions on the mechanical properties of the interface between the substrate and WAAM deposit.

- If the substrate is to be included in the part, then understanding and controlling the performance of the interface is critical.
- Using the same alloy for the WAAM deposit and substrate provides a uniform chemical composition, provided that no significant alloying element losses are generated. In as-deposited condition, the WAAM deposit performances are lower than

the substrate. Using the same alloy makes possible the global heat treatment of the component, as the solution treatment temperature is chemical composition dependent.
- When using different alloys, there is a significant variation of chemical composition across the interface. In the case of the 2024 alloy investigated here, this caused the formation of microstructural features, accelerating crack propagation in the second deposited layer. However, dilution by solute atoms, in this case, magnesium, from the substrate can enhance the strength and hardness of the interfacial region.
- Heat treatment can be beneficial for increasing and homogenising the properties at the interface, but compromises might be required when treating dissimilar alloy structures.
- Rolling is also beneficial because it reduces the gap in mechanical properties between the substrate and WAAM deposit. However, the rolling parameters need to be varied depending on the vicinity of a layer to the substrate to avoid localised weaknesses caused by un-closed pores and un-event microstructure in the first layers.
- RSA material as substrate can be beneficial because of the reduction/elimination of liquation below the fusion zone that weakened the WAAM deposit and substrate joint.

Funding

This research work was enabled by the financial support from C-TEC, Constellium Technology Center, and the Engineering and Physical Sciences Research Council (EPSRC) through the NewWire Additive Manufacturing (grant number EP/R027218/1) research programme.

CRediT authorship contribution statement

E. Eimer: Conceptualization, Investigation, Writing – original draft. **S. Williams:** Conceptualization, Resources, Writing – review & editing, Supervision. **J. Ding:** Conceptualization, Resources, Writing – review & editing, Supervision. **S. Ganguly:** Writing – review & editing. **B. Chehab:** Resources, Writing – review & editing, Supervision.

Declaration of Competing Interest

The authors declare the following financial interests/personal relationships which may be considered as potential competing interests: 'Eloise Eimer reports equipment, drugs, or supplies was provided by RSP technology.'

Acknowledgement

The author would like to thank RSP Technology for providing part of the raw material used in this study, and the reviewers for the constructive feedback they provided. The authors would also like to give their gratitude to Flemming Nielsen and Nisar Shar, who supported lab activities, and Steve Pope and Tracey Robert, who assisted with the metallurgical preparations at Cranfield University.

Data Availability Statement

The data underlying this study can be accessed through the Cranfield University repository at https://doi.org/10.17862/cranfield.rd.18858338

References

[1] M. Niino, Development of functionally gradient material, J. Jpn. Soc. Powder Powder Metall. 37 (2) (1990) 241–244.
[2] M.R. Modupe, A.E. Titilayo, in: Functionally Graded Materials, Springer, 2017, https://doi.org/10.1016/b978-0-444-82548-3.x5000-8.
[3] D.C. Hofmann, S. Roberts, R. Otis, J. Kolodziejska, R.P. Dillon, J.O. Suh, et al., Developing gradient metal alloys through radial deposition additive manufacturing, Sci. Rep. (2014) 4, https://doi.org/10.1038/srep05357.
[4] D.C. Hofmann, J. Kolodziejska, S. Roberts, R. Otis, R.P. Dillon, J.O. Suh, et al., Compositionally graded metals: a new frontier of additive manufacturing, J. Mater. Res. 29 (17) (2014) 1899–1910, https://doi.org/10.1557/jmr.2014.208.
[5] G. Marinelli, F. Martina, H. Lewtas, D. Hancock, S. Ganguly, S. Williams, Functionally graded structures of refractory metals by wire arc additive manufacturing, Sci. Technol. Weld. Joining Taylor & Francis 24 (5) (2019) 495–503, doi: 10.1080/13621718.2019.1586162.
[6] L. Thivillon, P. Bertrand, B. Laget, I. Smurov, Potential of direct metal deposition technology for manufacturing thick functionally graded coatings and parts for reactors components Elsevier B.V., J. Nucl. Mater. 385 (2) (2009) 236–241, https://doi.org/10.1016/j.jnucmat.2008.11.023.
[7] M. Merklein, R. Schulte, T. Papke, An innovative process combination of additive manufacturing and sheet bulk metal forming for manufacturing a functional hybrid part Elsevier B.V., J. Mater. Processing Technol. 291 (2021), https://doi.org/10.1016/j.jmatprotec.2020.117032 117032.
[8] E.A. Starke, J.T. Staleyt, Application of modern aluminum alloys to aircraft, Prog. Aerosp. Sci. 32 (95) (1996) 131–172, https://doi.org/10.1016/0376-0421(95)00004–6.
[9] S.W. Williams, F. Martina, A.C. Addison, J. Ding, G. Pardal, P. Colegrove, Wire +Arc additive manufacturing, Mater. Sci. Technol. 32 (7) (2016) 641–647, https://doi.org/10.1179/1743284715Y.0000000073.
[10] J. Ding, P. Colegrove, F. Martina, S. Williams, R. Wiktorowicz, M.R. Palt, Development of a laminar flow local shielding device for wire+arc additive manufacture, J. Mater. Processing Technol. Elsevier B.V. 226 (2015) 99–105, https://doi.org/10.1016/j.jmatprotec.2015.07.005.
[11] H. Lockett, J. Ding, S. Williams, F. Martina, Design for Wire + Arc Additive Manufacture: design rules and build orientation selection, J. Eng. Des. 4828 (2017) 1–31, doi: 10.1080/09544828.2017.1365826
[12] J. Zhang, X. Wang, S. Paddea, X. Zhang, Fatigue crack propagation behaviour in wire + arc additive manufactured Ti - 6Al - 4V: effects of microstructure and residual stress Elsevier Ltd, Mater. Des. 90 (2015) 551–561, https://doi.org/10.1016/j.matdes.2015.10.141.
[13] J. Gu, S. Yang, M. Gao, J. Bai, K. Liu, Influence of deposition strategy of structural interface on microstructures and mechanical properties of additively manufactured Al alloy Elsevier, Additive Manuf. 34 (January) (2020), https://doi.org/10.1016/j.addma.2020.101370 101370.
[14] E. Eimer, S. Williams, J. Ding, S. Ganguly, B. Chehab, Effect of substrate alloy type on the microstructure of the substrate and deposited material interface in aluminium wire + arc additive manufacturing, Metals. 11 (6) (2021), https://doi.org/10.3390/met11060916.
[15] J. Gu, J. Ding, S.W. Williams, H. Gu, J. Bai, Y. Zhai, et al., The strengthening effect of inter-layer cold working and post-deposition heat treatment on the additively manufactured Al– 6.3————————————————Cu alloy, J. Mater. Processing Technol. Elsevier 230 (2016) 26–34, doi: 10.1016/j.jmatprotec.2015.11.006 (Accessed: 14 April 2016).
[16] J. Gu, J. Ding, S.W. Williams, H. Gu, P. Ma, Y. Zhai, The effect of inter-layer cold working and post-deposition heat treatment on porosity in additively manufactured aluminum alloys, J. Mater. Process. Technol. 230 (2016) 26–34, https://doi.org/10.1016/j.jmatprotec.2015.11.006.
[17] K.F. Ayarkwa, S. Williams, J. Ding, Investigation of pulse advance cold metal transfer on aluminium wire arc additive manufacturing, Int. J. Rapid Manuf. 5 (1) (2015) 44–57.
[18] J.Y. Bai, C.L. Yang, S.B. Lin, B.L. Dong, C.L. Fan, Mechanical properties of 2219-Al components produced by additive manufacturing with TIG, Int. J. Adv. Manuf. Technol. 86 (1–4) (2015) 479–485, https://doi.org/10.1007/s00170-015-8168-x.
[19] C.A. Brice, N. Dennis, Cooling rate determination in additively manufactured aluminum alloy 2219, Metall. Mater. Trans. A 46 (5) (2015) 2304–2308, https://doi.org/10.1007/s11661-015-2775-x.
[20] E.M. Ryan, T.J. Sabin, J.F. Watts, M.J. Whiting, The influence of build parameters and wire batch on porosity of wire and arc additive manufactured aluminium alloy 2319 Elsevier, J. Mater. Processing Tech. 262 (July) (2018) 577–584, https://doi.org/10.1016/j.jmatprotec.2018.07.030.
[21] J.R. Honnige, P.A. Colegrove, S. Ganguly, E. Eimer, S. Kabra, S. Williams, Control of residual stress and distortion in aluminium wire + arc additive manufactured with rolling, Addit. Manuf. 22 (2018) 775–783, https://doi.org/10.1016/j.addma.2018.06.015.
[22] R. Bai, Y. Wei, Z. Lei, H. Jiang, W. Tao, C. Yan, et al., Local zone-wise elastic-plastic constitutive parameters of Laser-welded aluminium alloy 6061 using digital image correlation Elsevier Ltd, Optics Lasers Eng. 101 (May 2017) (2018) 28–34, https://doi.org/10.1016/j.optlaseng.2017.09.023.
[23] S. Kou, Precipitation-Hardening Materials I: Aluminium Alloys. Welding Metallurgy, second ed., John Wiley & Sons, Inc., Hoboken, NJ, USA, 2003, doi: 10.1002/0471434027 (Accessed: 19 January 2016).
[24] C. Huang, G. Cao, S. Kou, Liquation cracking in partial penetration aluminium welds: assessing tendencies to liquate, crack and backfill, Sci. Technol. Weld.

Joining 9 (2) (2004) 149–156, doi: 10.1179/136217104225017071 (Accessed: 14 January 2016).
[25] C. Huang, S. Kou, Liquation mechanisms in multicomponent aluminum alloys during welding, Weld. Res. (2002) 211–222.
[26] K.S. Rao, G.M. Reddy, K.P. Rao, Studies on partially melted zone in aluminium-copper alloy welds - effect of techniques and prior thermal temper, Mater. Sci. Eng. A 403 (1–2) (2005) 69–76, https://doi.org/10.1016/j.msea.2005.04.041.
[27] C.G. Pickin, S.W. Williams, P.B. Prangnell, J. Robson, M. Lunt, Control of weld composition when welding high strength aluminium alloy using the tandem process, Sci. Technol. Weld. Join. 14 (8) (2009) 734–739, https://doi.org/10.1179/136217109X12505932584817.
[28] C.G. Pickin, S.W. Williams, P.B. Prangnell, J. Robson, M. Lunt, C. Derry, et al., Control of weld composition when arc welding high strength aluminium alloys using multiple filler wires, Sci. Technol. Weld. Join. 15 (6) (2010) 491–496, https://doi.org/10.1179/136217110X12785889549660.
[29] S. Kou, A simple index for predicting the susceptibility to solidification cracking, Weld. J. 94 (December) (2015) 374–388.
[30] N/A. Military Handbook - MIL-HDBK-5H: Metallic Materials and Elements for Aerospace Vehicle Structures. U.S. Department of Defense, 1998. Available from: <https://app.knovel.com/hotlink/toc/id:kpMHMILH61/military-handbook-mil/military-handbook-mil>.
[31] RSP Technology. RS Alloys Overview. Available from: <http://www.rsp-technology.com/site-media/user-uploads/rsp_alloys_overview_2018lr.pdf> (Accessed: 30 October 2018)
[32] The Aluminum Association Inc. International Alloy Designations and Chemical Composition Limits for Wrought Aluminum and Wrought Aluminum Alloys, Arlington, 2009.
[33] B. Cong, J. Ding, S. Williams, Effect of arc mode in cold metal transfer process on porosity of additively manufactured Al-6.3%Cu alloy, Int. J. Adv. Manuf. Technol. 76 (9–12) (2015) 1593–1606, https://doi.org/10.1007/s00170-014-6346-x.
[34] Z. Pinter, Study of Aluminium Wire + Arc Additive Manufacture, Cranfield University, UK, 2017.
[35] S.D. Dumolt, D.E. Laughlin, J.C. Williams, The effect of welding on the microstructure of the age hardening Aluminum alloy 2219, in: First Int. Alum. Weld. Conf. Cleveland, Ohio, 1981, pp. 115–1. Available from: <https://www.andrew.cmu.edu/user/dl0p/laughlin/pdf/030.pdf>.
[36] J. Gu, J. Bai, J. Ding, S. Williams, L. Wang, K. Liu, Design and cracking susceptibility of additively manufactured Al-Cu-Mg alloys with tandem wires and pulsed arc Elsevier, J. Mater. Processing Technol. 262 (May) (2018) 210–220, https://doi.org/10.1016/j.jmatprotec.2018.06.030.